Chapter 8
Contrails and contrail cirrus

8.1 Introduction - Terminology

8.2 Contrail formation conditions

8.3 Heterogeneous nucleation on volatile aerosol and soot

8.4 Indirect effect of soot on cirrus

8.5 Contrail cirrus

8.6 Variability of contrail properties

8.7 Heterogeneous chemistry on contrails

8.8 Aerodynamic contrails

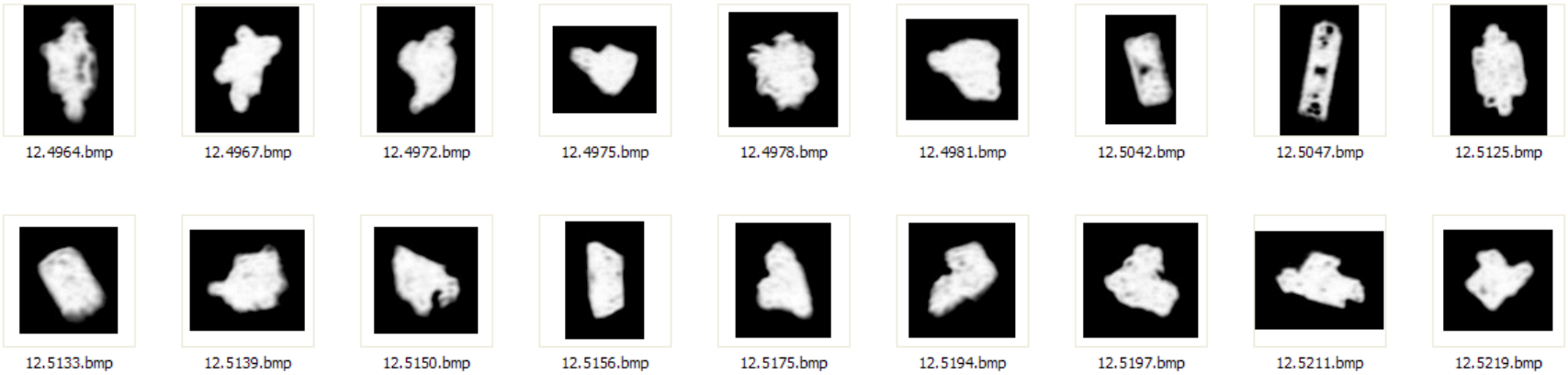

Gayet, 2008, A380

Detection of the contrail of an A380

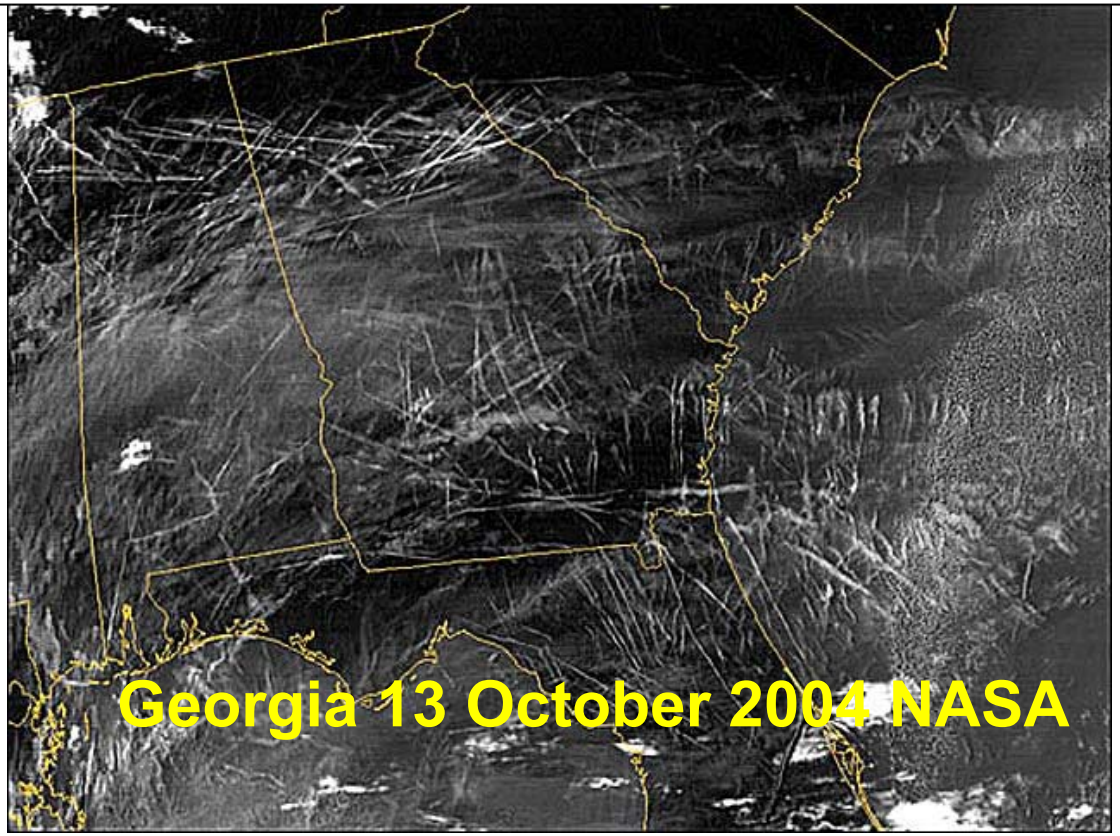

Introduction

• Contrails develop at lower relative humidity than natural cirrus and therefore can modify high cloudiness.

• Contrails change the radiation budget and the upper tropospheric moisture budget significantly.

Introduction 2

• Aircraft influence high clouds directly by producing line-shaped contrails.

• Contrails can persist and spread in ice-supersaturated air. The resulting clusters of contrail-cirrus can be observed on regional scales, sometimes also in regions without significant air traffic, because they are advected with the wind field over large distances.

Introduction 3

• Contrails predominantly form when aircraft fly through preexisting cirrus clouds, sometimes accompanied by the formation of distrails. The main effect seems to be the formation of a localized 'cloud hole':

Introduction 4

• Aircraft influence high clouds indirectly by injecting aerosol particles that may act as heterogeneous ice nuclei at some point after emission. In the absence of aircraft emissions, a cirrus cloud would not have formed or the resulting cirrus would have different properties.

• It is important to recognize that a strong coupling may exist between the pure direct and indirect effects.

• Contrail-cirrus can exert an indirect effect on their own. Cirrus may have different properties because they nucleate in regions with preexisting ice and share the available water.

Chapter 8
Contrails and contrail cirrus

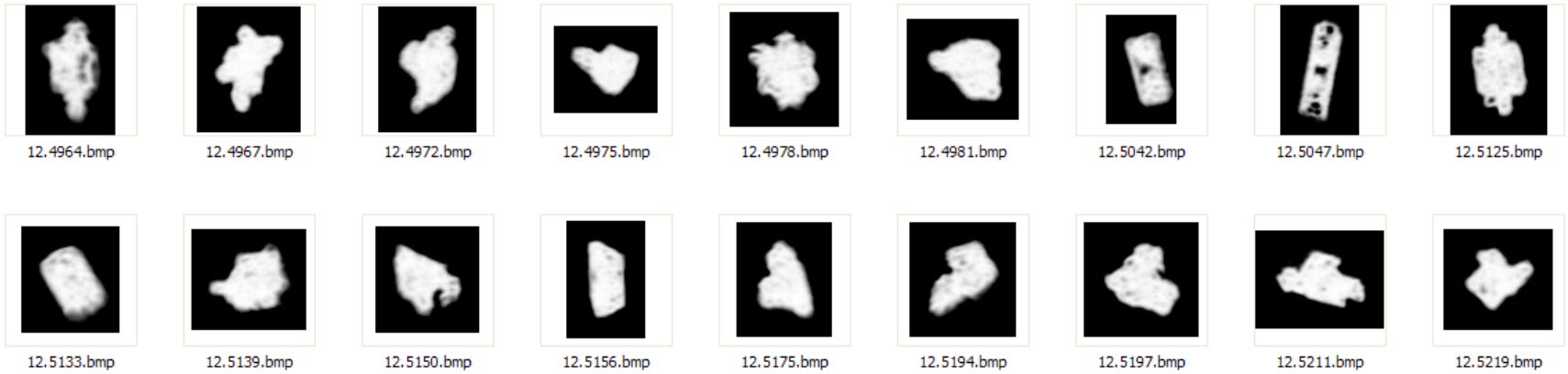

Gayet, 2008, A380

7.7.1 Formation conditions of contrails

• Contrails consist of ice particles that nucleate primarily on aerosols emitted or formed in the plume.

• At initial stage contrails grow by deposition of exhaust water vapor.

• Later during their life cycle contrails grow by deposition of entrained ambient water vapor.

• Formation of contrails due to increase in RHI during isobaric mixing of the hot and humid exhaust gases with colder and less humid ambient air.

• Contrail formation within ~ a wingspan distance behind the aircraft when S with respect to water is reached.

• Threshold temperatures and humidities for contrail formation at a given flight level are directly specified by thermodynamic relations.

8.2 Contrail formation conditions

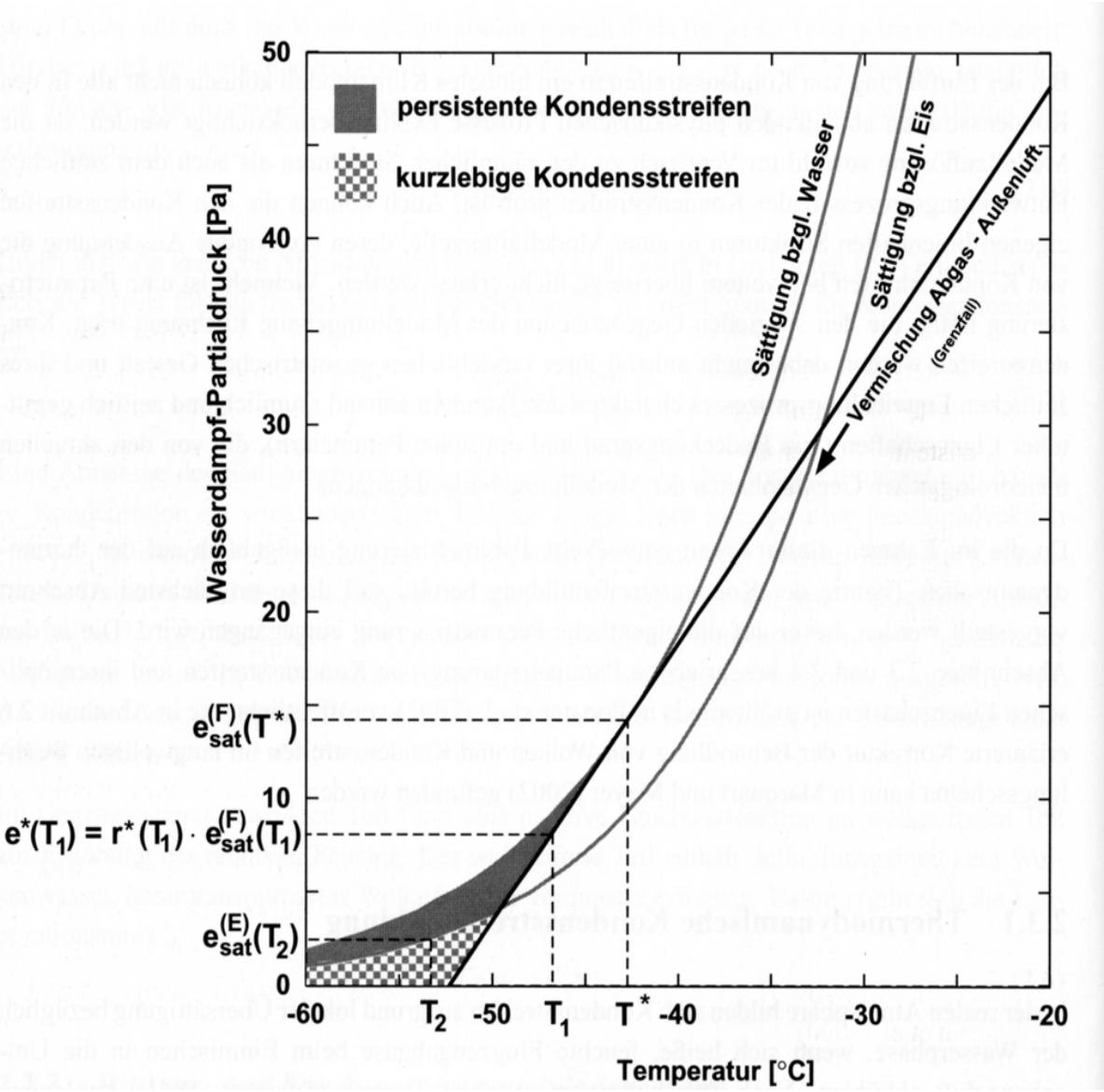

Chapter 8
Contrails and contrail cirrus

8.3 Homogeneous nucleation of contrails in volatile aerosol

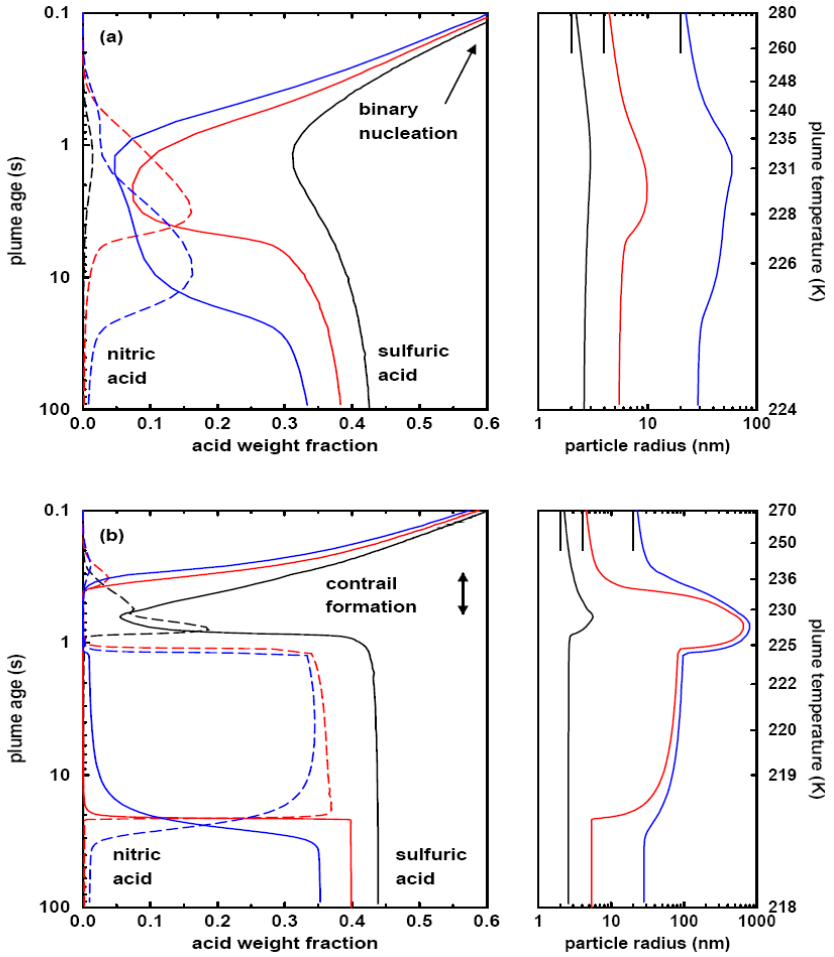

Volatile and soot exhaust aerosol are processed by rapid uptake of H2O and H2SO4 in contrails. Ice crystals that scavenged sulfate aerosols release larger sulfate droplets upon evaporation.

Kärcher, 1999

8.3 Heterogeneous nucleation of contrails on soot

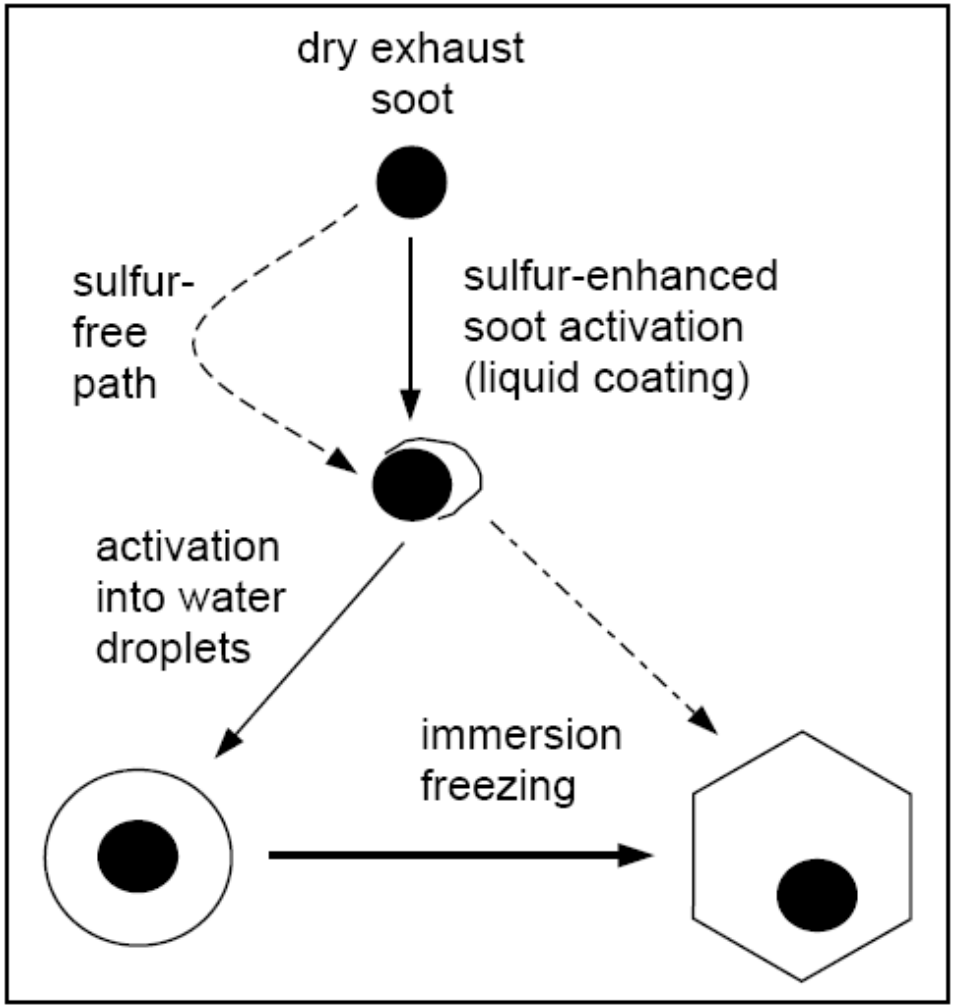

Kärcher, 1998

8.3 Heterogeneous nucleation of contrails on soot and volatile aerosol

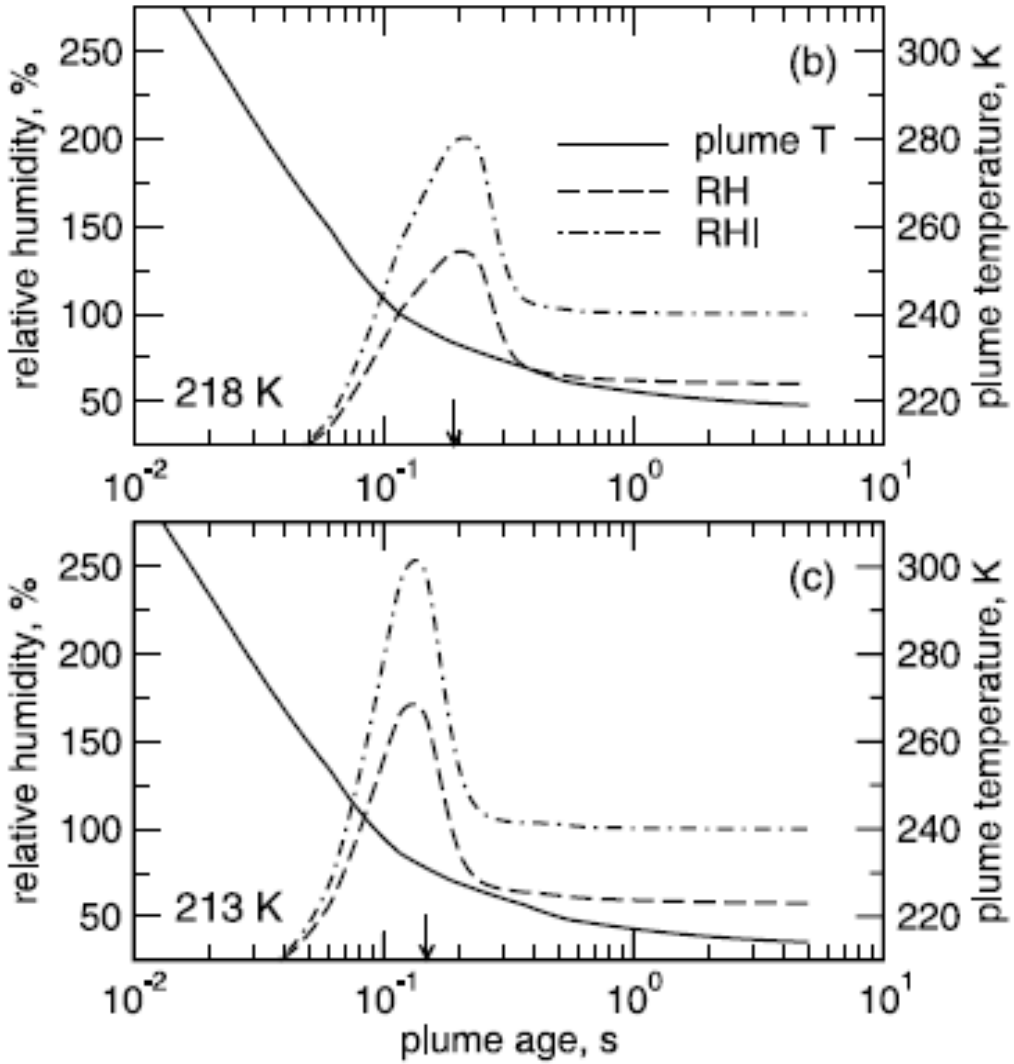

after Kärcher and Yu, 2009

8.3 Heterogeneous nucleation of contrails on soot and volatile aerosol

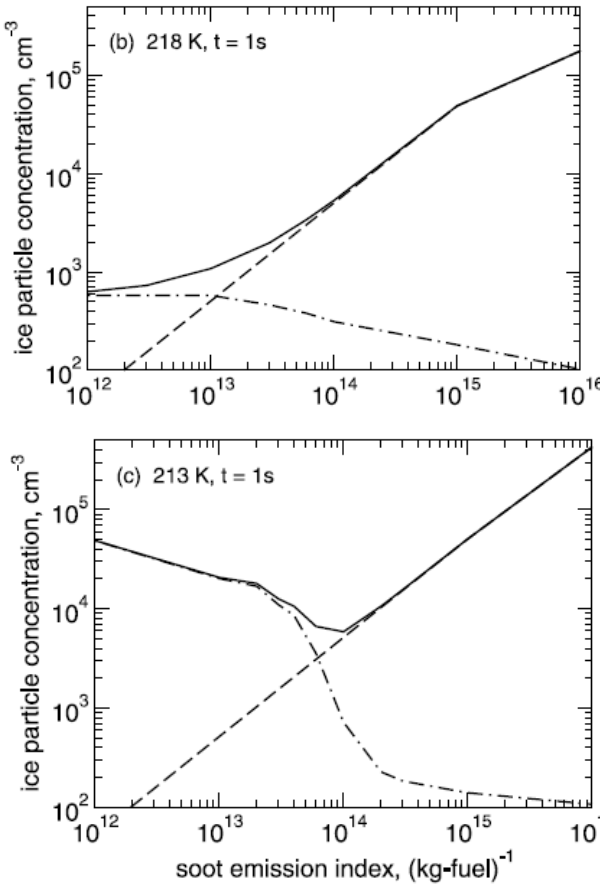

Chapter 8
Contrails and contrail cirrus

8.4 Indirect effect of soot on cirrus

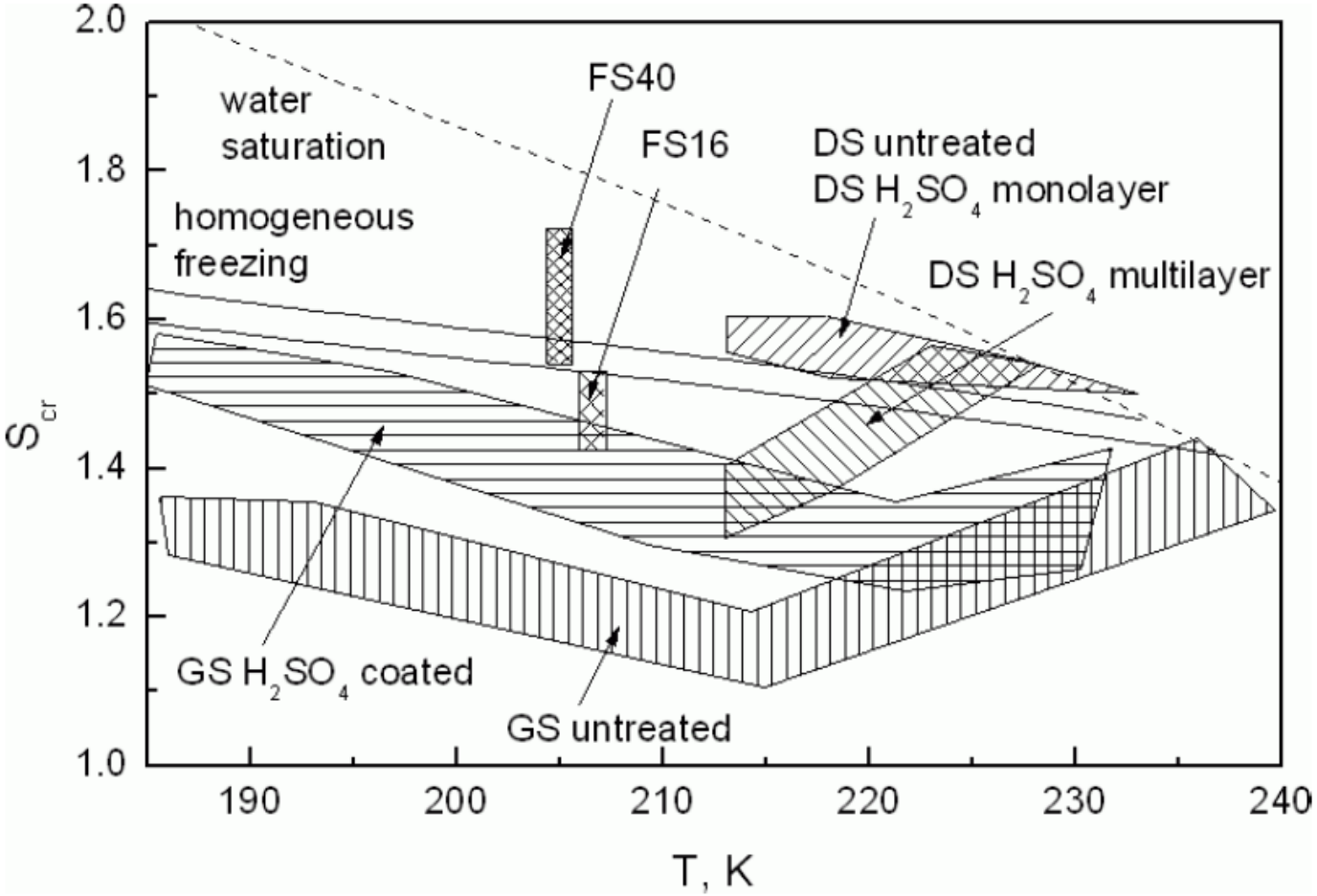

Kärcher et al., ACP, 2007

8.4 Indirect effect of soot on cirrus

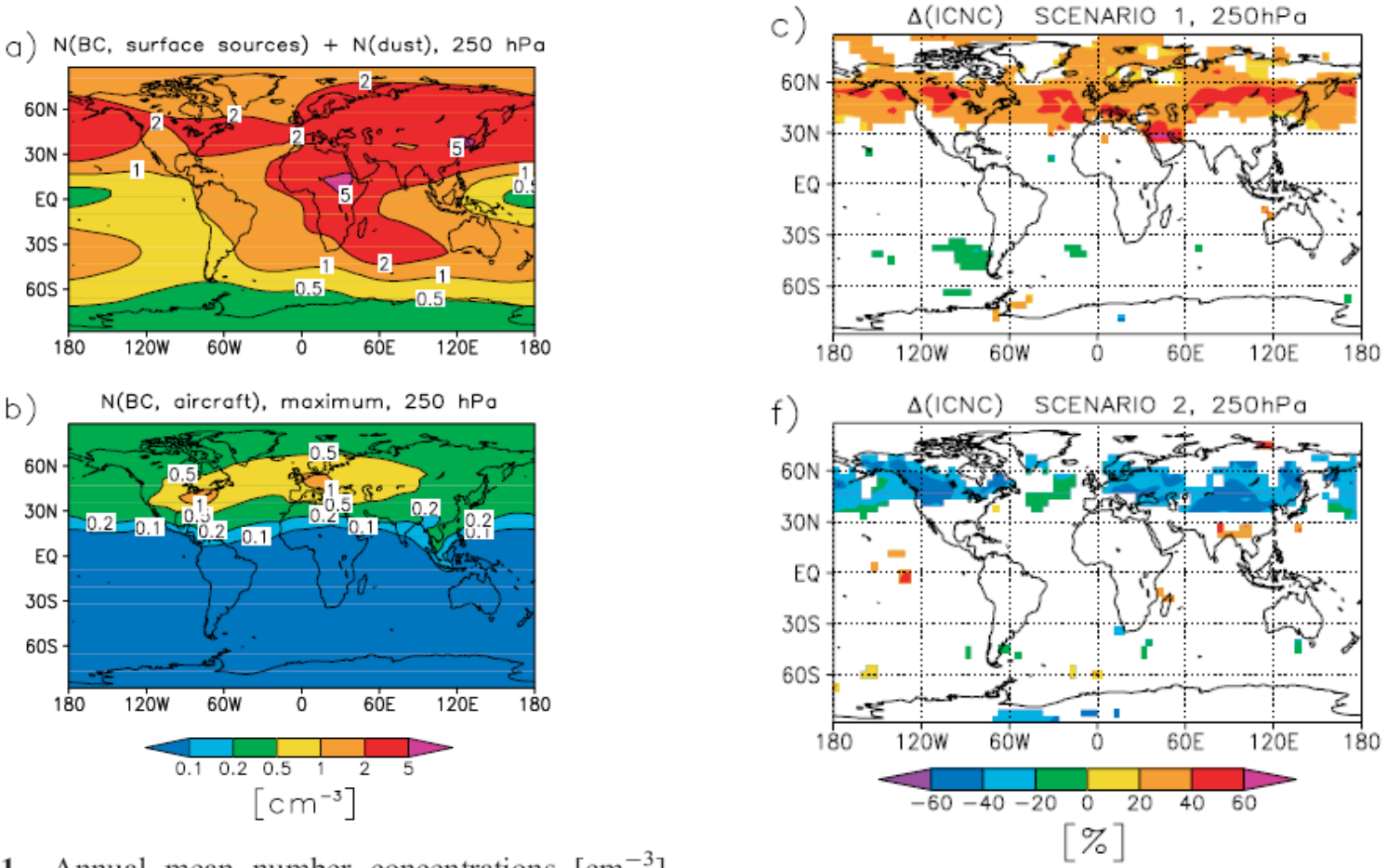

Figure 1. Annual mean number concentrations [cm^{-3}] of potential IN at 250 hPa (main aircraft flight level). (a) Hydrophilic BC and mineral dust particles originating from surface sources. (b) BC particles from aircraft (maximum estimate by *Hendricks et al.* [2004]). The results were taken from the HOM simulation.

Hendricks et al., GRL, 2005

Chapter 8
Contrails and contrail cirrus

8.5 Growth of ice crystals in contrails

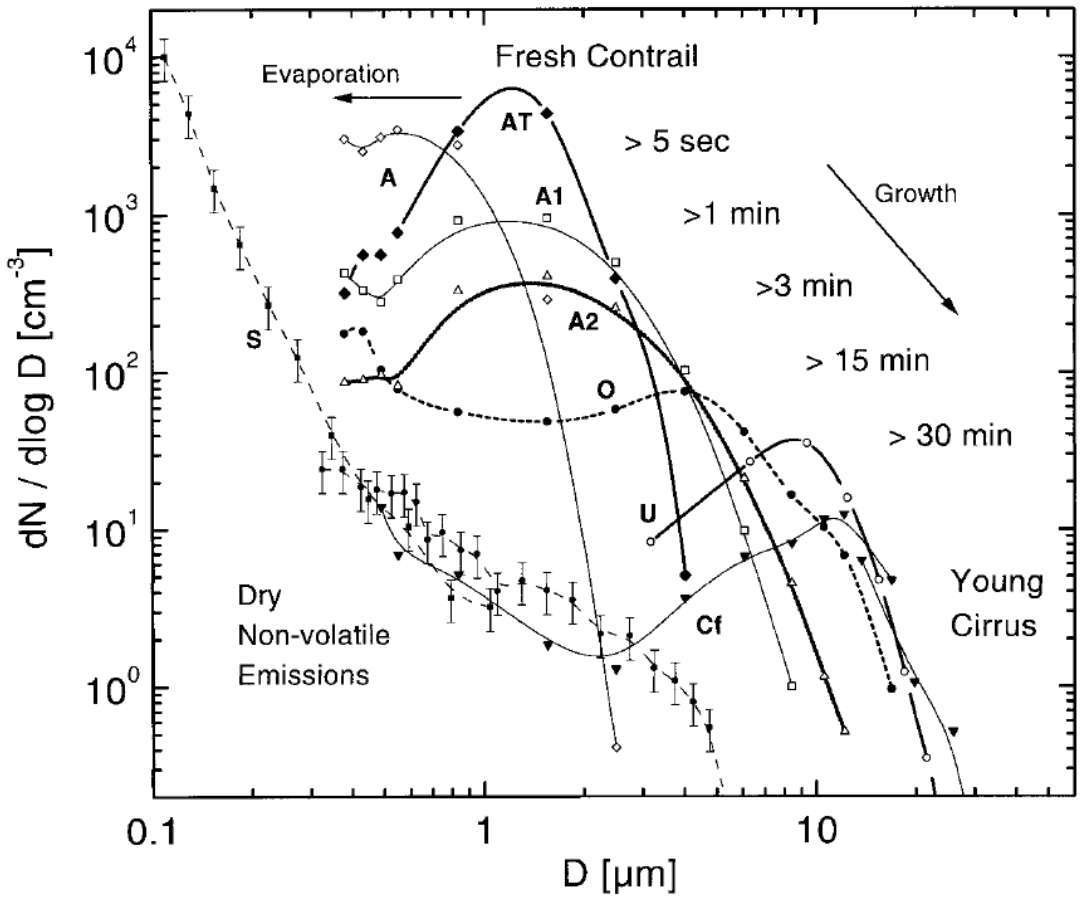

FIG. 1. Representative selection of particle concentrations illustrating the transition of contrails into cirrus clouds. Contrail cases: AT (solid diamonds), A (open diamonds, solid line), A1 (open squares, solid line), A2 (open triangles, bold dotted), O (solid circles, dashed), and U (open circles, bold line); case Cf: young cirrus cloud (solid triangles, solid line); case S: dry exhaust jet aircraft emissions (combined PCASP and FSSP-300 spectra; solid squares and circles, respectively). Error bars added to S mark the typical measurement uncertainty range of 30% representative for all distributions. For more details, see text.

Schröder et al., 1999

8.5 Growth of ice crystals in contrails - transition into contrail cirrus

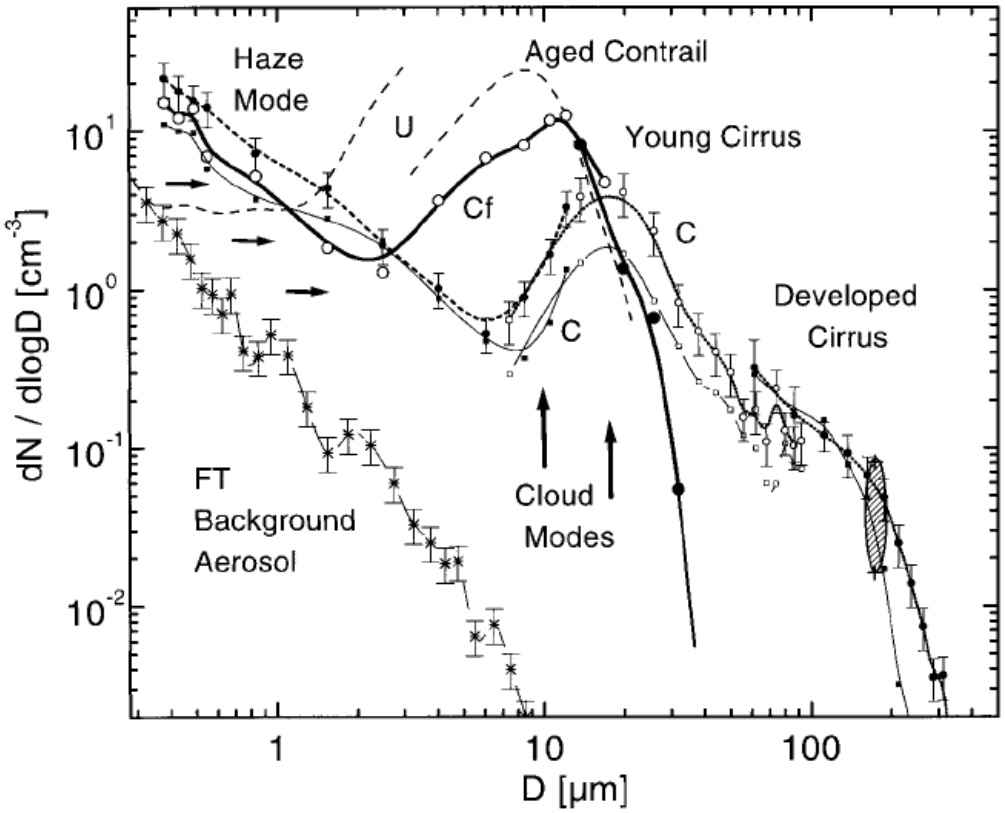

FIG. 4. Comparison of the size spectra of an aged contrail (U, no symbols, dashed lines; derived from FSSP-100 and PCASP), a young cirrus (Cf), a developed cirrus cloud (C), and an atmospheric background aerosol distribution (FT). Case Cf: large circles, bold line, open symbols for FSSP-300, solid symbols for FSSP-100ER; case C: two distributions (small open symbols for FSSP-100 data, small solid symbols for FSSP-300 and OAP data) representing an approximate range of variability inside dense regions of the developed cirrus; case FT: star symbols, represents the actual free tropospheric background aerosol (averaged over several min) in the wider vicinity of C and Cf. Representative 30% error bars are added to one distribution of C and to FT. A comparison with REP-derived crystal concentration (>80–100 μm diameter) is given by the large ellipsoid. Potential hygroscopic growth of background aerosols toward the coarse mode is indicated by short horizontal arrows. The mean mode diameter position of Cf and C is shown by upward-pointing arrows. For further interpretation, see text.

Schröder et al., 1999

8.5 Growth of ice crystals in contrails - transition into contrail cirrus

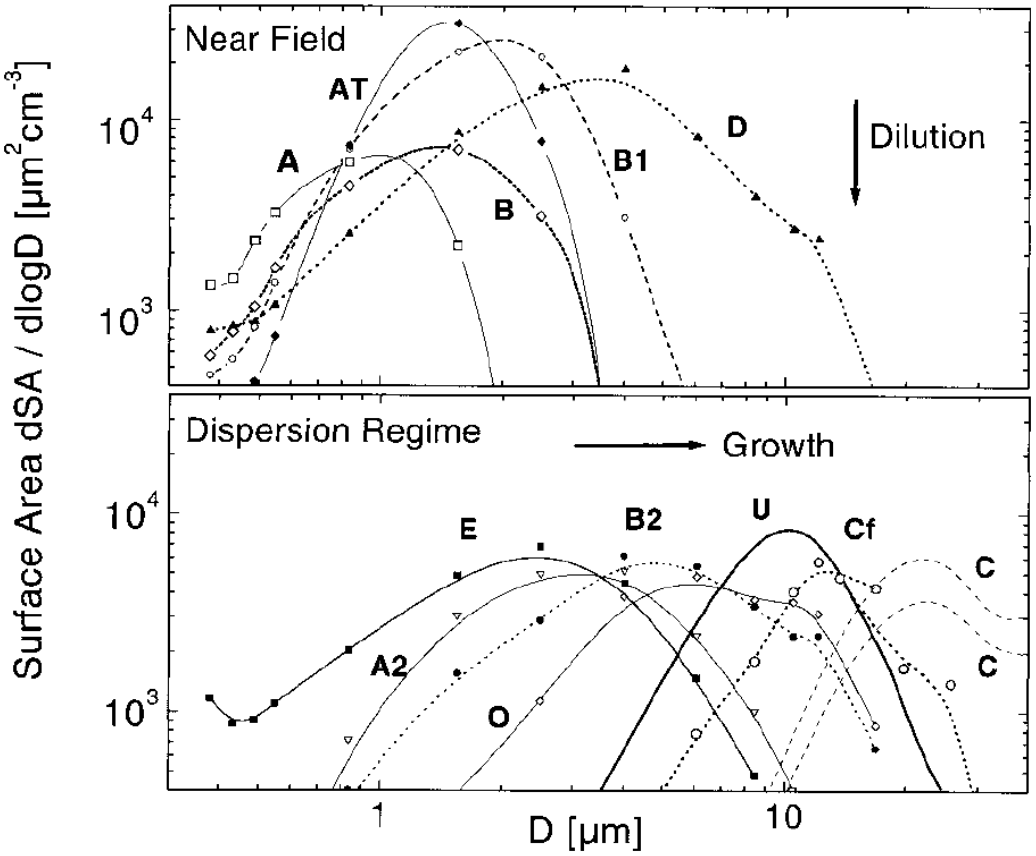

FIG. 7. Evolution of ice crystal surface area distributions inside aging contrails. (upper) Near-field distributions, showing the effect of plume dilution on the spectra: A (open squares, solid line), B (open diamonds, dotted), AT (solid diamonds, solid line), B1 (open circles, dashed), D (solid triangles, dotted). (lower) Dispersion regime contrails and cirrus clouds, showing crystal growth during the transformation of contrail into young cirrus clouds: E (solid squares, solid

Schröder et al., 1999

8.5 Transition of contrails into contrail cirrus

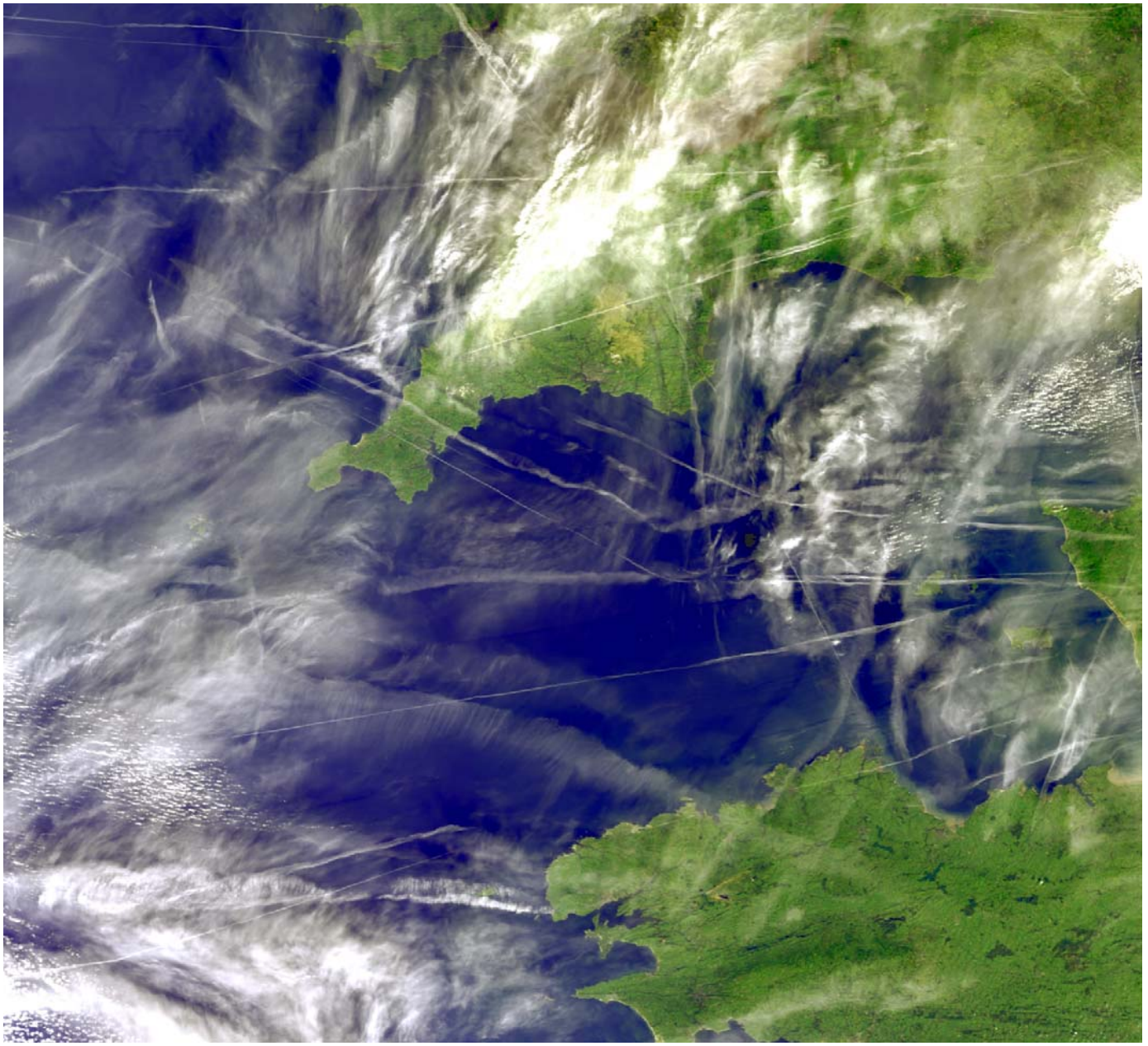

8.5 Simulation of contrail cirrus coverage

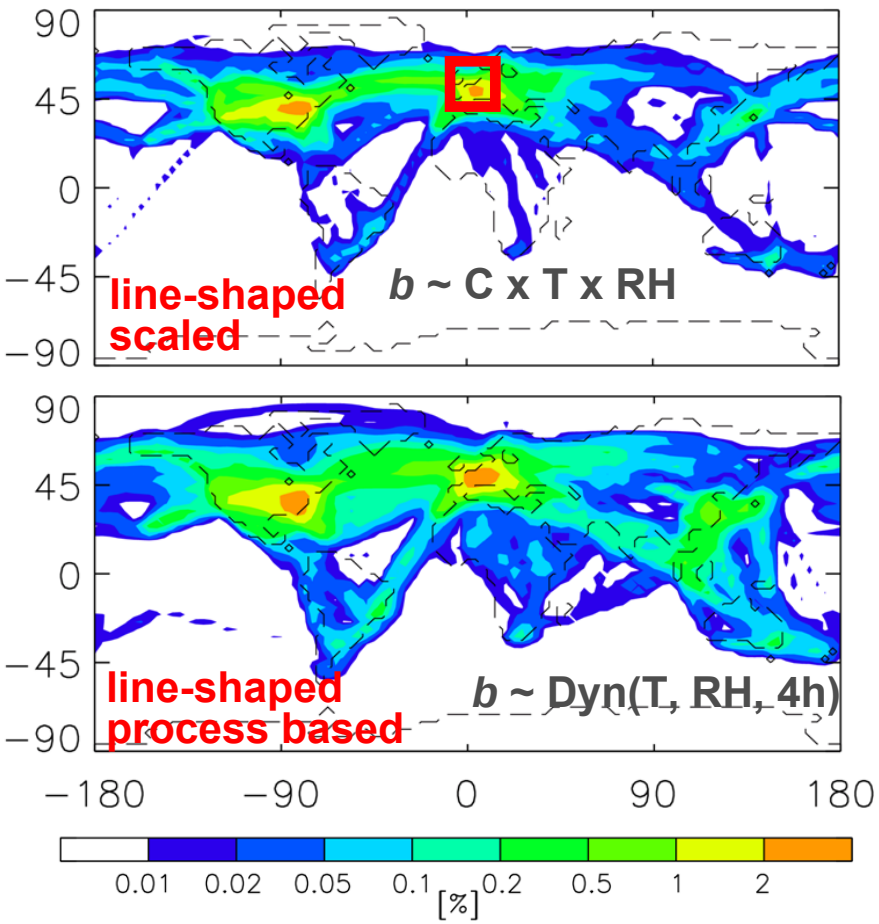

logarithmic scale

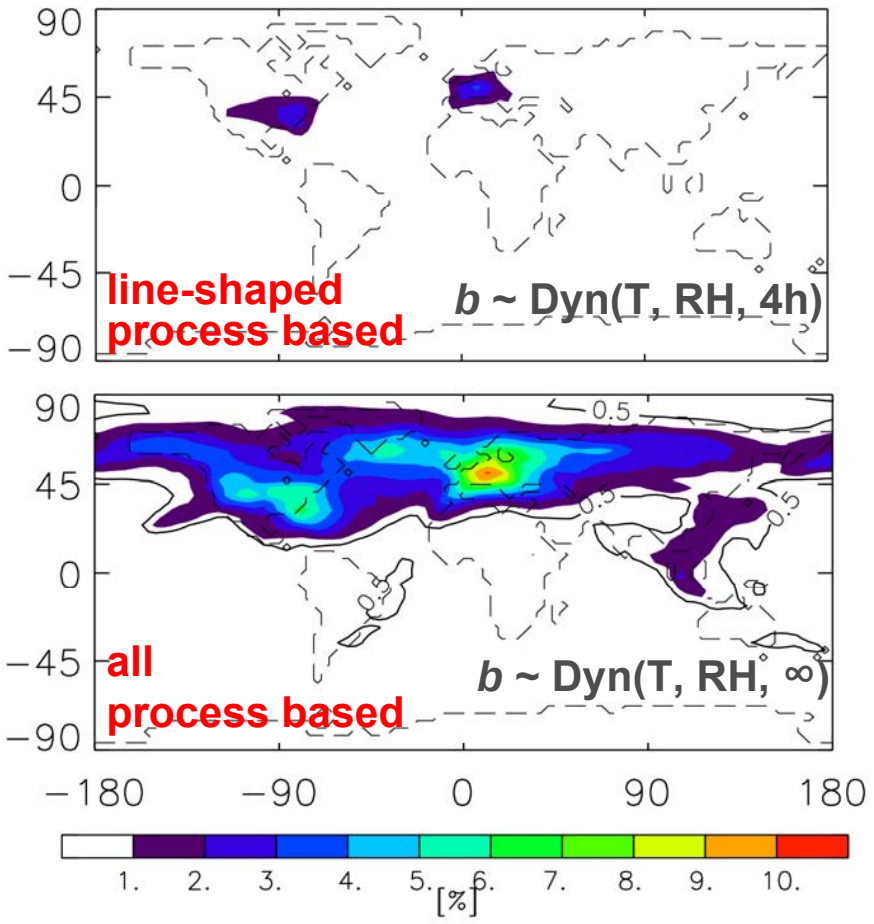

linear scale

8.5 Simulation of contrail cirrus coverage

	line-shaped contrails		contrail cirrus	
	visible	all	visible	all
new scheme	0.05	0.10	0.50	1.14

Increase in coverage due to ageing contrails regionally very variable

Increase depends on visibility threshold and overlap assumptions

Chapter 8
Contrails and contrail cirrus

8.6 Variability of contrail cirrus properties-

Interannual variability of contrail coverage

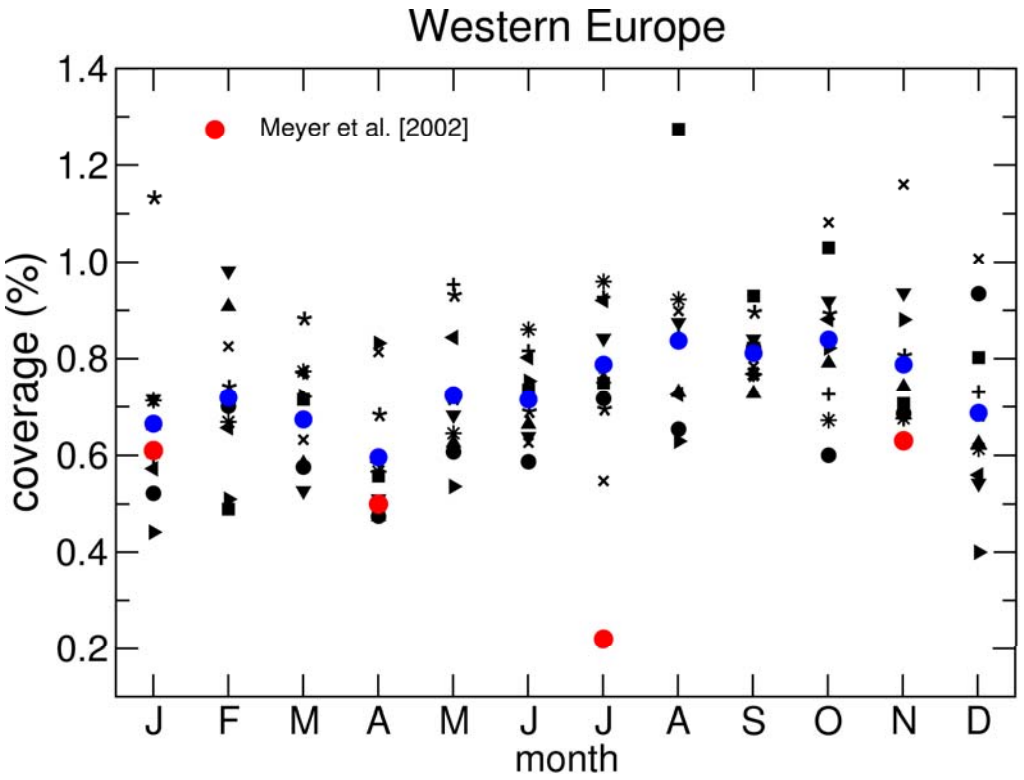

observations

model realizations

model average

Burkhardt and Kärcher, JGR, 2009

8.6 Variability of contrail cirrus optical depth

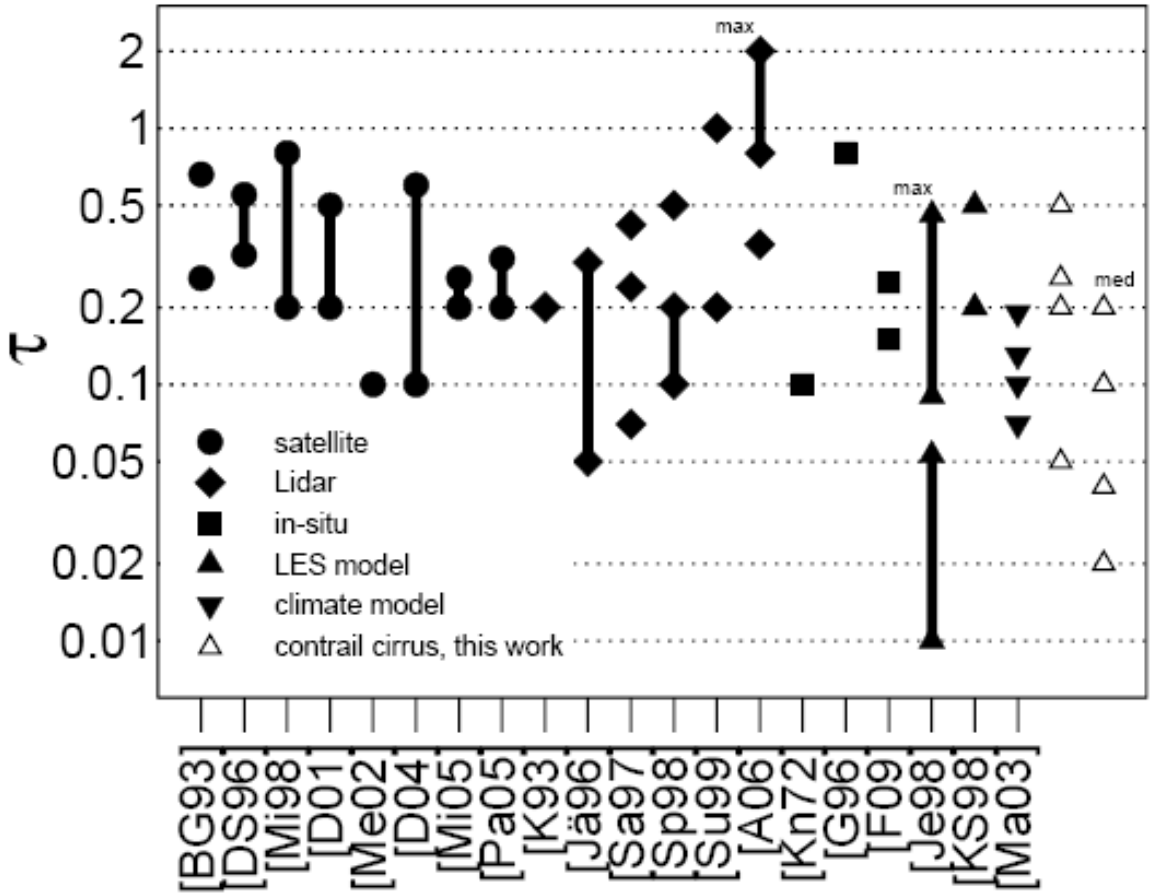

Fig. 8. Compilation of visible optical depths for observed and modeled persistent, line-shaped contrails from various sources. Data points represent mean values except when labelled "max" (maximum) or "med" (median). Open symbols are values for contrail cirrus from Tables 3 and 4. Several issues preclude a full intercomparability of the data, see text.

8.6 Variability of contrail cirrus properties

Aircraft contrails develop into contrail cirrus by depositional growth and sedimentation of ice particles and horizontal spreading due to wind shear. Factors controlling this development include temperature, ice supersaturation, thickness of ice-supersaturated layers, and vertical gradients in the horizontal wind field.

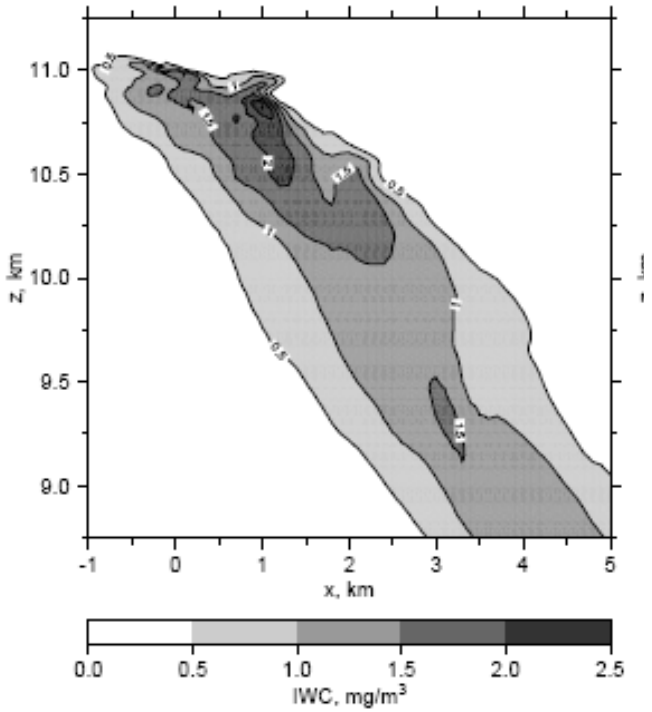

Fig. 1. Distribution of ice water content in an optically thin contrail cirrus cloud of age 2 h from (left) LES and (right) the CCSIM. In the LES, the initial IWC distribution was obtained from a simulation of the vortex phase evolution of the contrail and covered a region 300×150 m centered at $z = 11$ km and $x = 0$ km. In the CCSIM, the initial IWC was homogeneously distributed

Kärcher et al., ACPD, 2009

8.6 Variability of contrail cirrus properties

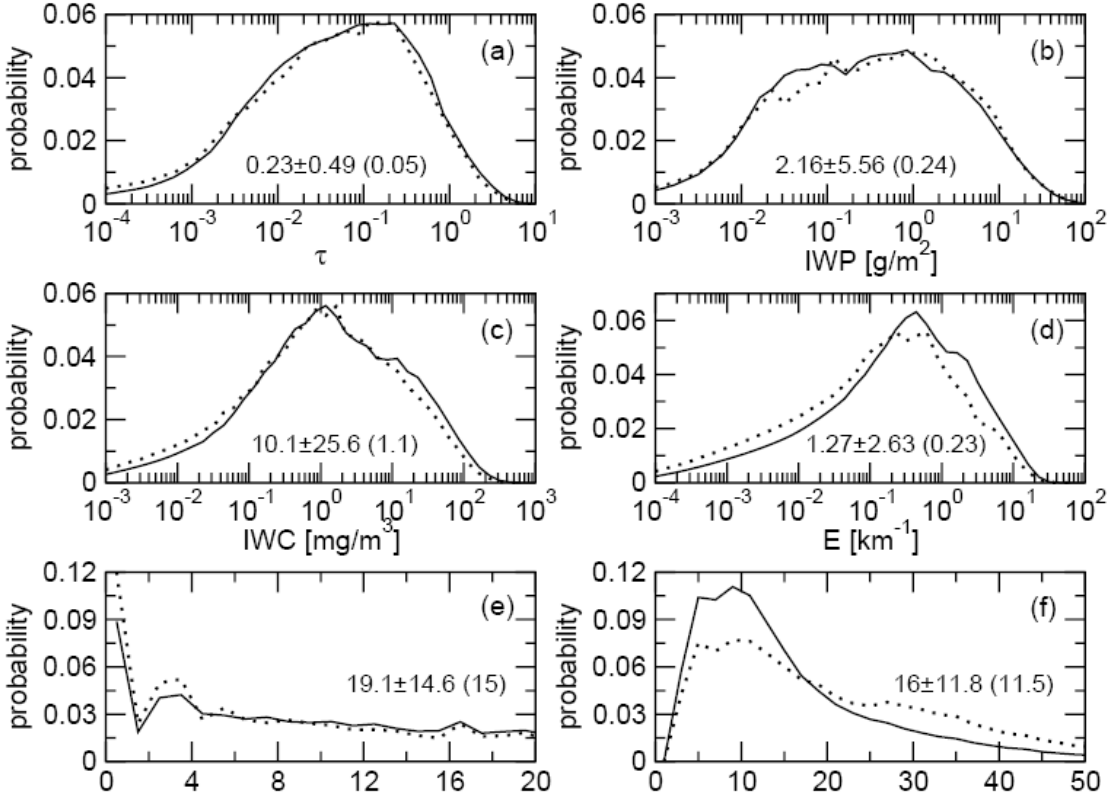

Fig. 10. Probability distributions of contrail cirrus **(a)** optical depth τ, **(b)** ice water paths IWP, **(c)** ice water contents IWC, **(d)** visible extinction E, **(e)** widths b, and **(f)** effective ice crystal radii r_{reff}. Values in each panel denote the distribution mean and standard deviation (median). The PDFs (solid curves) have been obtained by imposing simultaneous variability in temperature T, shear σ, ice supersaturation s, and supersaturated layer thickness d using the PDFs from Sect. 2.2.1. The set of dotted curves assumes a constant supersaturated layer thickness with the same mean value. Parameters are T_m=223±4 K, σ_m=0.0025 s^{-1} and c=1.2, s_m=0.1, and d_m=1 km, as suggested by the RUC analysis for 2001 over the continental USA. All simulations further used uniform random sampling of initial ice particle number density n_0 (average 30 cm^{-3}) and Gamma distributions with initial mean ice crystal radii $\bar{r}_0$ (average 1 μm) according to Eqs. (29) and (30) with φ_n=1.

8.6 Variability of contrail cirrus optical depth

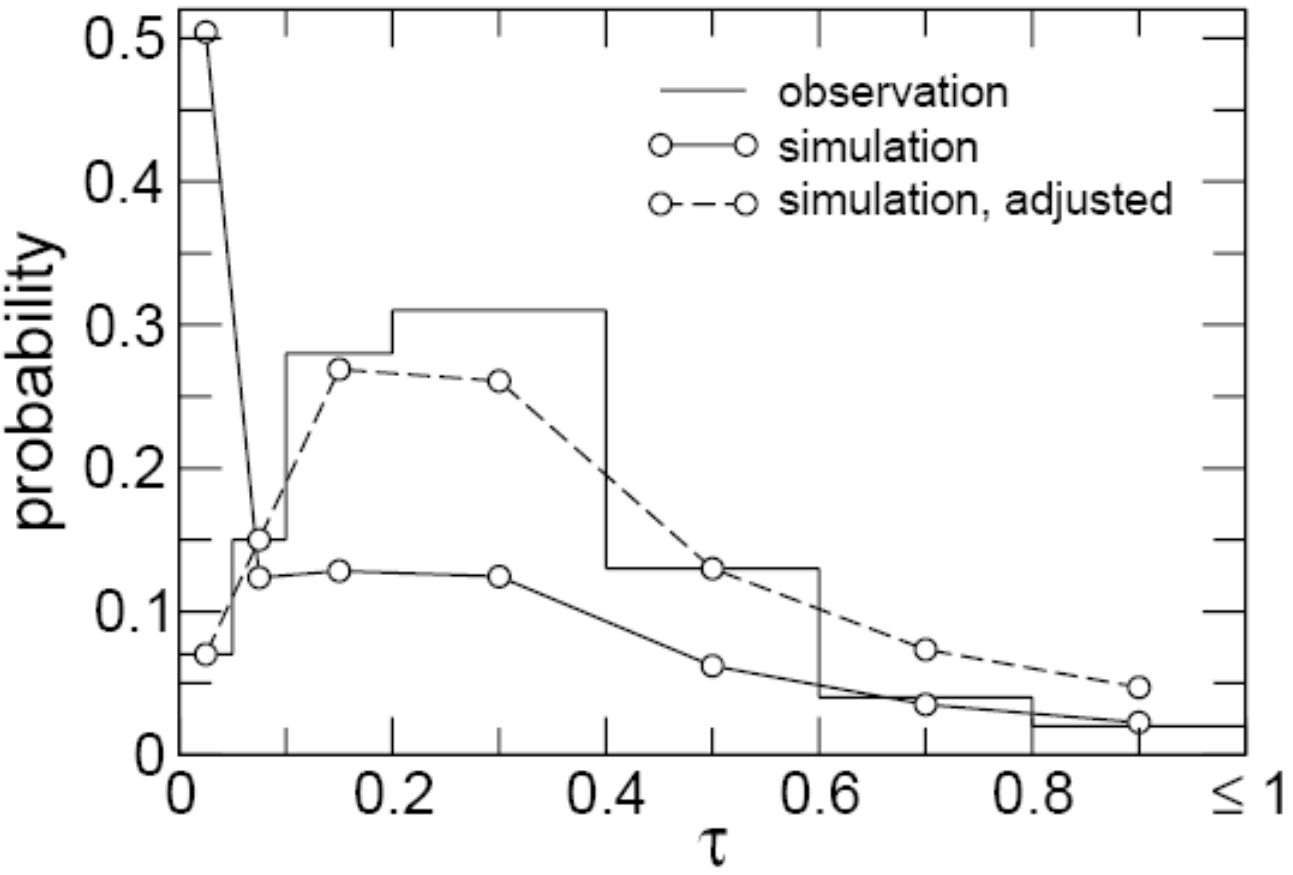

Fig. 9. Observed PDF of line-shaped persistent contrails (stepped lines), simulated PDF (solid curve) and simulated PDF adjusted with empirical detection efficiencies in the first two optical depth bins (dashed curve). Open circles mark the bin center values. For details, see text.

Kärcher et al., ACPD, 2009

Chapter 8
Contrails and contrail cirrus

8.7 Heterogeneous chemistry on contrails
Ozone changes due to aircraft emissions

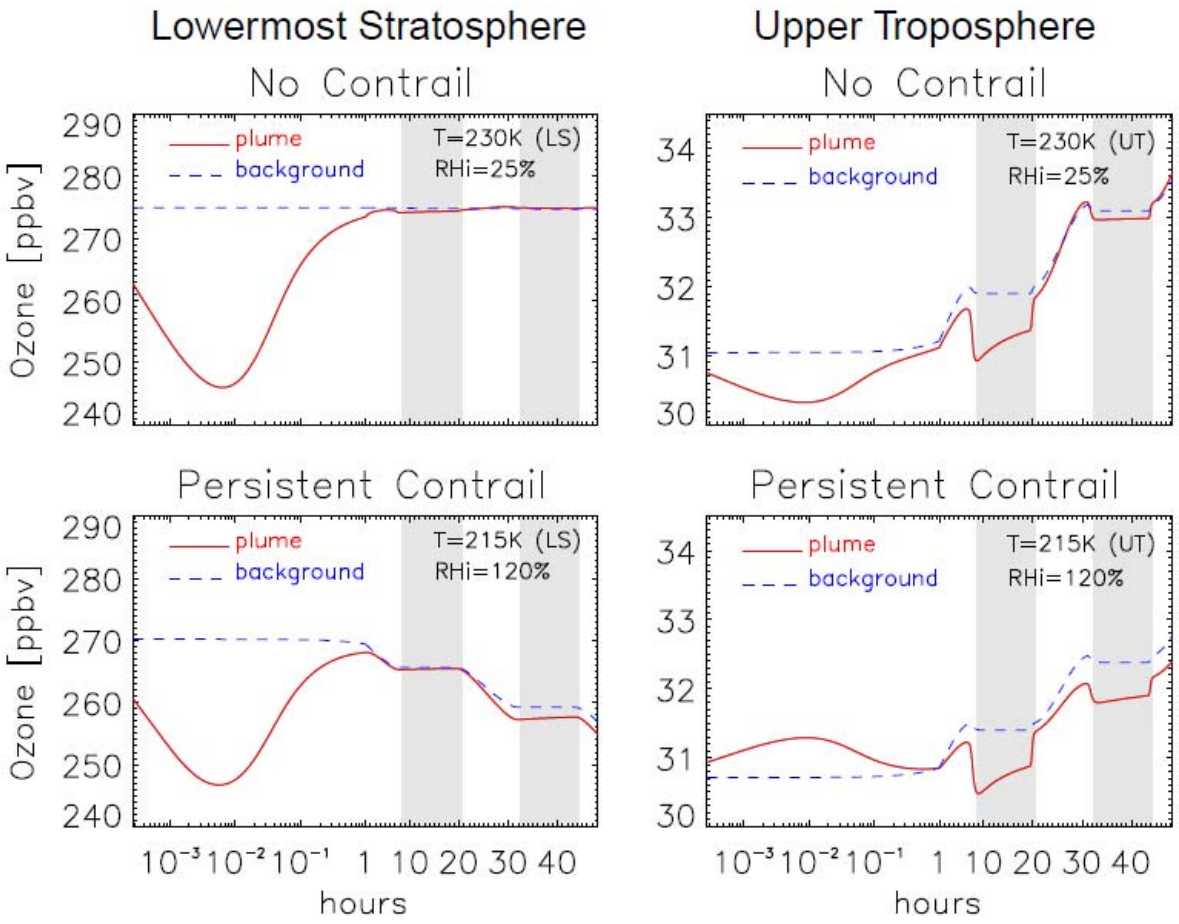

Fig. 4. Ozone concentrations along the plume axis, shown as a function of plume age for emissions into the lowermost stratosphere (left) and upper troposphere (right) considering cases of contrail (lower panels) and of non-contrail (upper panels) formation. Same conditions as in Fig. 3. The white and shaded areas indicate day and night.

Meilinger et al., ACP, 2005

8.7 Heterogeneous chemistry on contrails

Potential of aircraft aerosols and contrails to produce or destroy ozone

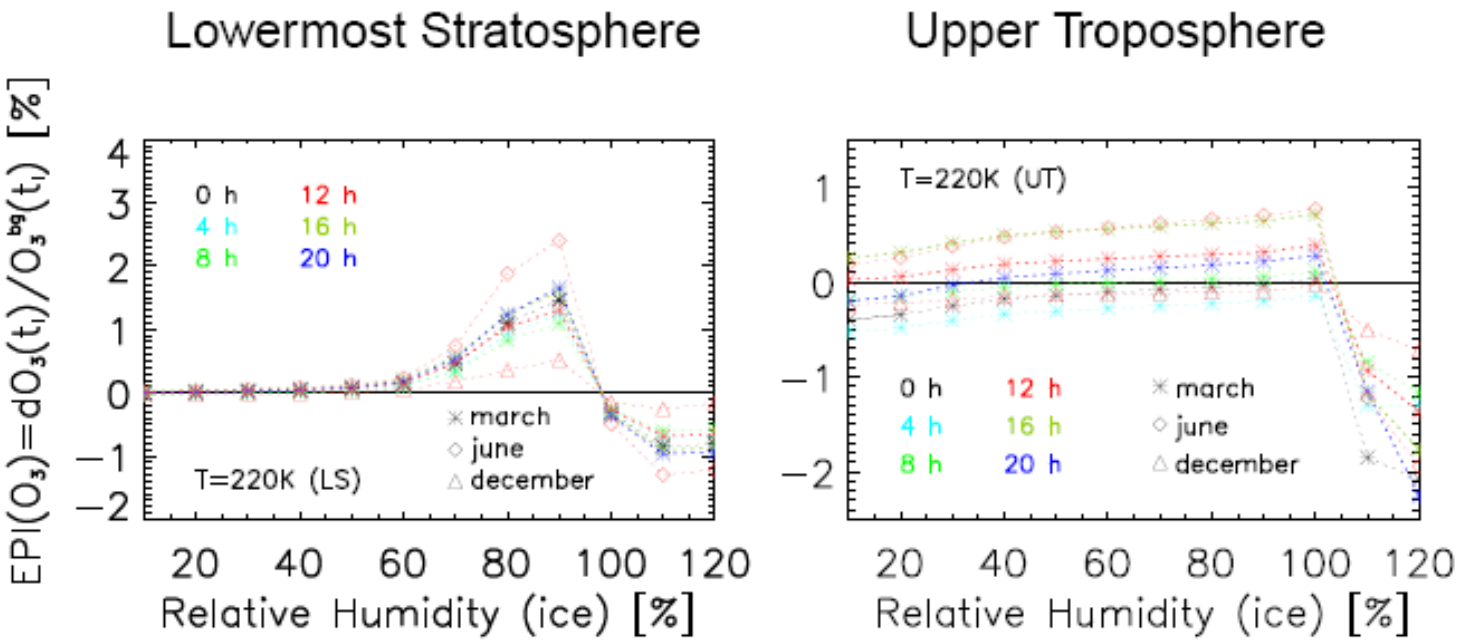

Fig. 8. Effective perturbation index of ozone for the NAFC as a function of RH_{ice}. Times (marked by different colors) indicate local times of emission. Same conditions as in Fig. 7.

Meilinger et al., ACP, 2005

Chapter 8
Contrails and contrail cirrus

8.1 Introduction - Terminology

8.2 Contrail formation conditions

8.3 Heterogeneous nucleation on volatile aerosol and soot

8.4 Indirect effect of soot on cirrus

8.5 Contrail cirrus

8.6 Variability of contrail properties

8.7 Heterogeneous chemistry on contrails

8.8 Aerodynamic contrails

8.8 Aerodynamic contrails

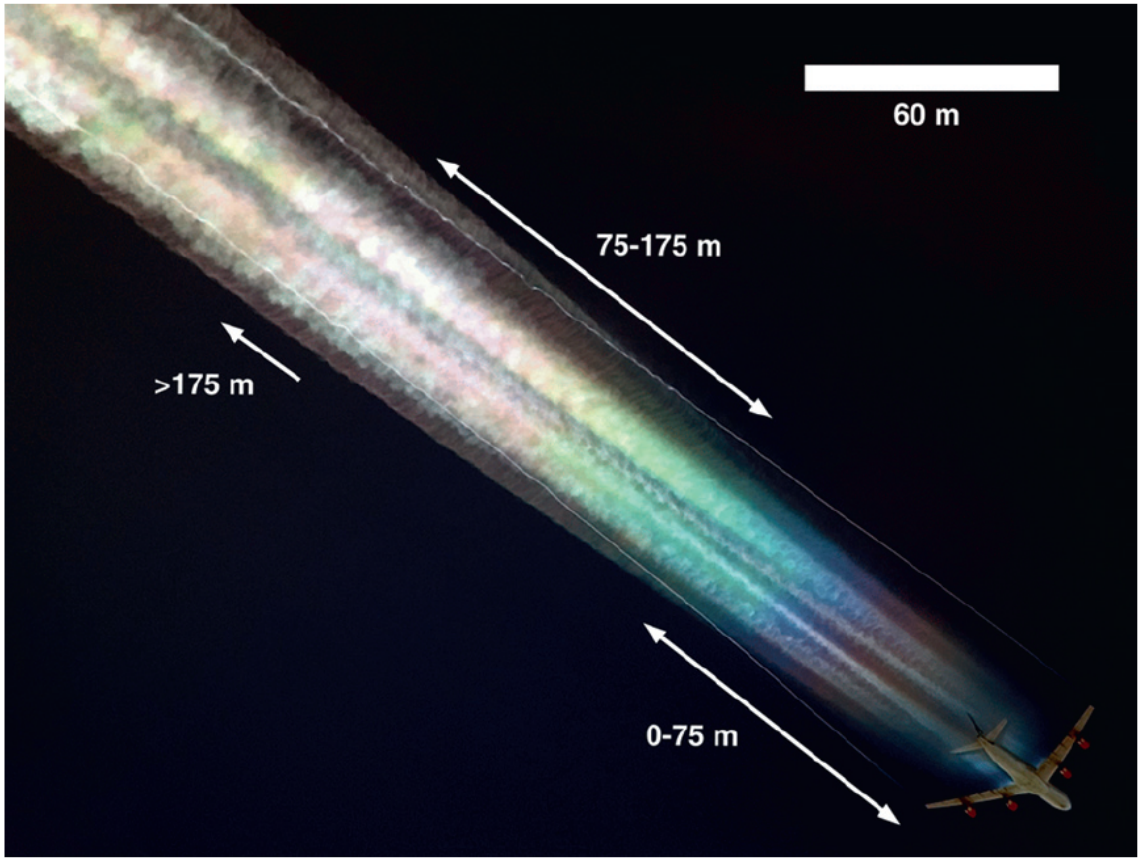

FIG. 1. Photograph of a contrail-producing Airbus A340 aircraft cruising at 9600-m altitude, close to a pressure level of 300 mb and a temperature of 241 K as estimated from NCEP reanalysis data. The photo was taken from a second aircraft 1200 m below on the same route over eastern China on 12 Jun 2005, from 1459 to 1506 Bejing time (~0700 UTC). Both aircraft were heading NW from 32°14.8′N, 119°46.7′E to 32°56.8′N, 119°10.1′E. The white bar marks the length scale, guided by the wing span (~60 m) of the airliner. Its wing depth is ~11 m. Any length scale can be converted to approximate times using a typical cruising speed of 250 m s^{-1} (e.g., 60 m corresponds to 0.24 s). The arrows and associated distances mark distinct color regimes appearing after the wing (blue/violet, green/yellow, pink/white). [Photo adapted from http://www.airliners.net/ courtesy of pilot Jeff Well (2007, personal communication).]

Gierens et al., JAS, 2009, Kärcher et al., JAS, 2009

8.8 Aerodynamic contrails

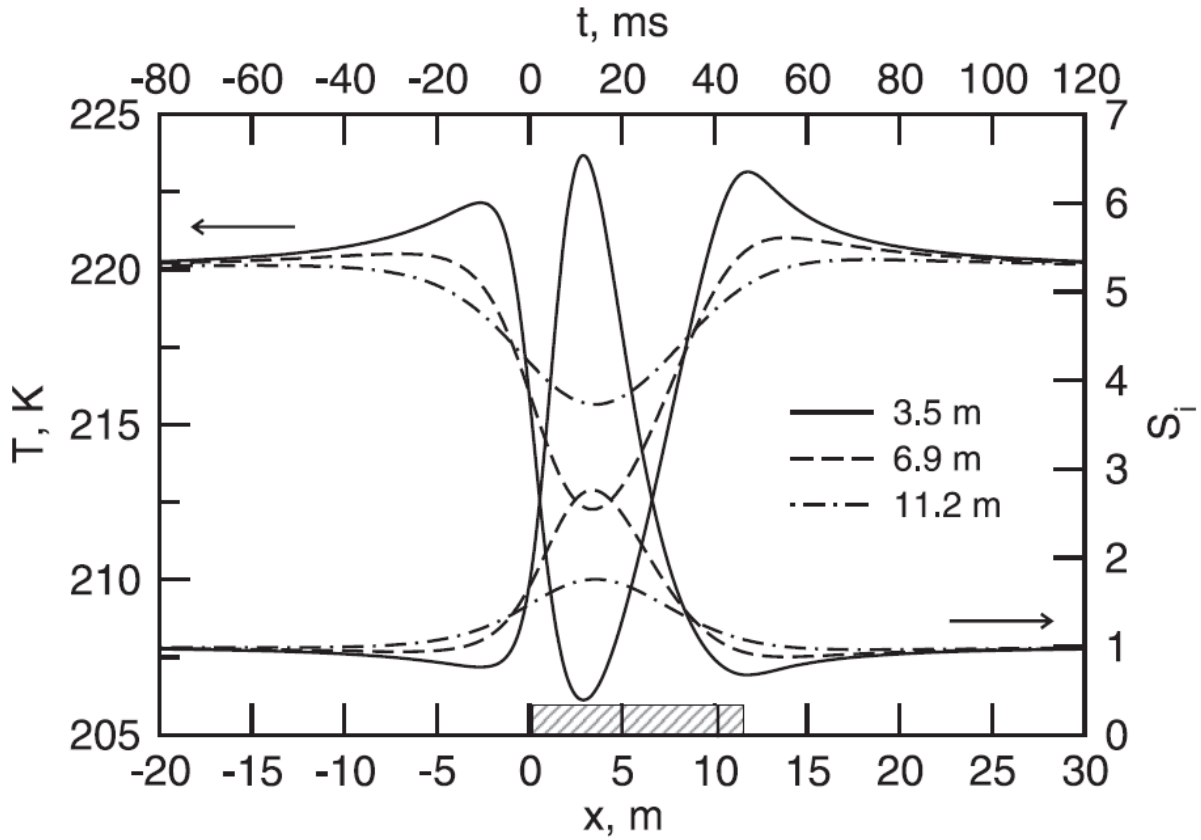

Gierens et al., JAS, 2009, Kärcher et al., JAS, 2009

8.8 Aerodynamic contrails

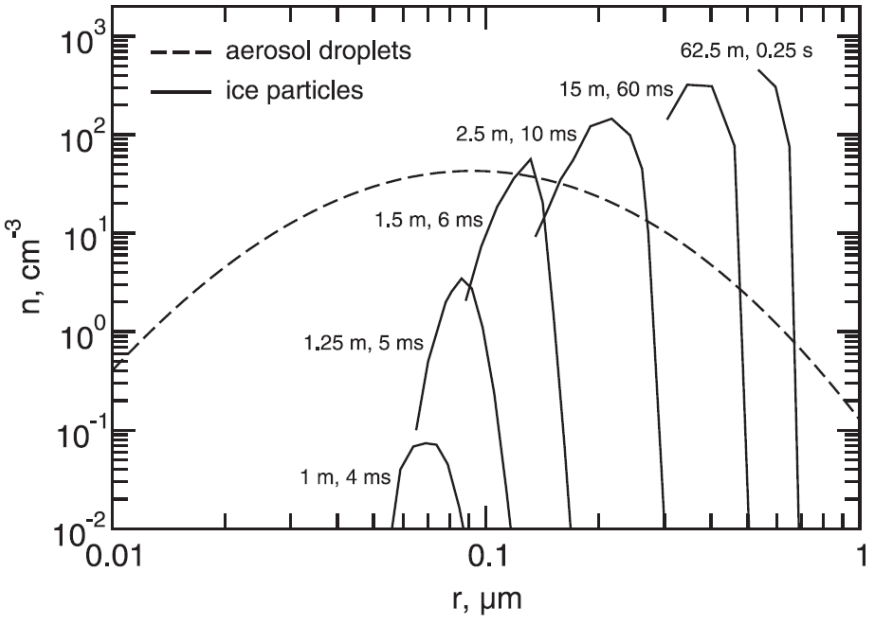

FIG. 6. Size distributions of aerosol (dashed) and ice particles (solid) along the trajectory located ~3.2 m above the wing corresponding to Fig. 5. The initial wet aerosol size spectrum is shown along with selected ice crystal spectra. Labels on the latter indicate distances past the leading edge of the wing and corresponding times elapsed.

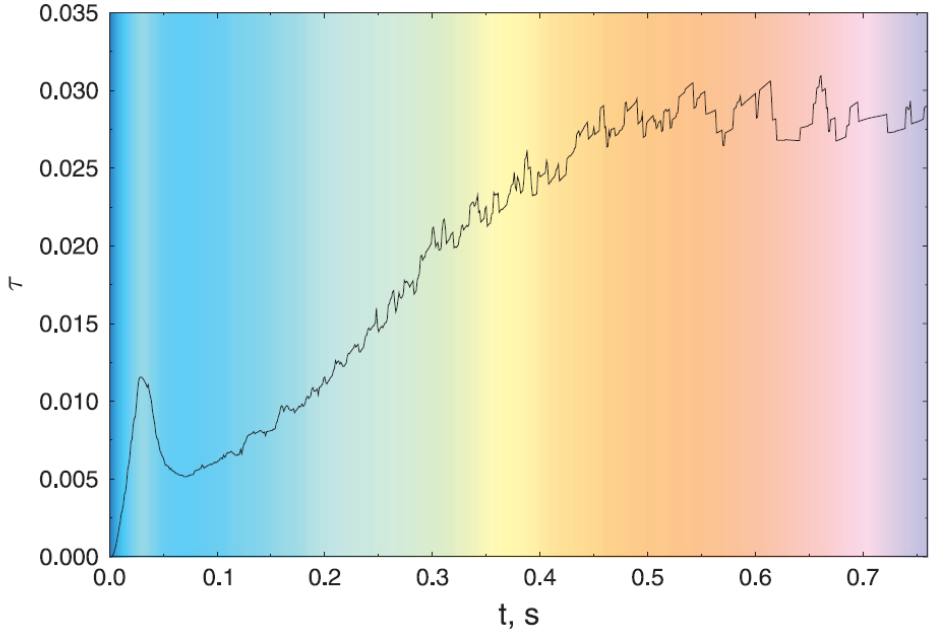

FIG. 7. Evolution of visible optical depth τ_v and the appearance of colors as a function of time t after the air has passed the leading edge of the wing. Color sequence can be compared to Fig. 1.